Oceanologia, 67 (3)/2025, 67304
Polish Academy of Sciences
Institute of Oceanology

https://doi.org/10.5697/ATWF9251

Fluorescence characteristics of dissolved organic matter and its association with the nepheloid layer in the northern South China Sea

Xiaochao Sui[1], Li Zou[1,*], Tian Chen[2], Yinuo Wang[1], Chaoqi Zhu[2], Yonggang Jia[2]

Abstract
The northern South China Sea (SCS) is characterized by multiple oceanographic phenomena and has developed diverse patterns of distribution, migration and transformation of dissolved organic carbon (DOC). To better understand the DOC behavior and its relationship with the nepheloid layer, UV-visible absorption spectra and three- dimensional fluorescence spectra of dissolved organic matter (DOM) were obtained in the northern SCS, as well as beam attenuation (BA), major physicochemical parameters and chlorophyll *a* (Chl-*a*) data. DOC and chromophoric dissolved organic matter (CDOM) gradually decrease from the surface to deeper layers, with high-low alternations occurring in the euphotic zone. The fluorescence intensity of DOM is primarily attributed to protein-like components, followed by humic-like components (24.6%). CDOM exhibits a typical marine origin and is produced mainly through bacterial production in situ. The spatial and temporal distributions of DOC and humic-like components are influenced by major physicochemical factors (such as temperature, salinity, and nutrients) and Chl-*a*. In contrast the protein-like components might be closely associated with bacterial activity. The distributions of DOC and humic-like components are significantly correlated with the presence of the nepheloid layer. In the euphotic zone, phytoplankton particulates are the primary source of humic-like components, while suspended particles affect the distribution of humic-like components below the euphotic zone. The results presented direct evidence for the function of the marine nepheloid layer in the organic carbon cycle.

Keywords
Northern South China Sea; Nepheloid layer; Dissolved organic carbon; FDOM

[1] *Key Laboratory of Marine Environmental Science and Ecology, Ministry of Education of China, Ocean University of China, Qingdao 266100, China*
[2] *Shandong Provincial Key Laboratory of Marine Environment and Geological Engineering, Ocean University of China, Qingdao 266100, China*
***Correspondence**: zouli@ouc.edu.cn (L. Zou)

Received: 25 December 2024; **revised:** 27 July 2025; **accepted**: 11 August 2025

1. Introduction

As the largest biologically active carbon reservoir in the ocean, dissolved organic carbon (DOC) is crucial in the marine carbon cycle (Hansell and Carlson, 1998). The global oceanic DOC reservoir contains 650 ± 30 Gt C (Hansell et al., 2012), equivalent to approximately 75% of the atmospheric CO_2 carbon inventory (880 ± 40 Gt C in 2021; Friedlingstein et al., 2022). This close order-of-magnitude relationship highlights DOC as a critical component in Earth's carbon cycle. Chromophoric dissolved organic matter (CDOM), an optically active fraction comprising 20–70% of the DOC pool with significantly higher proportions in oligotrophic open oceans than in eutrophic marginal seas (Coble, 1996; Jørgensen et al., 2011), interacts with solar radiation and exhibits a global distribution. CDOM sources display distinct regional patterns: autochthonous production dominates pelagic waters, contrasted by terrestrial dominance in coastal zones (Yamashita and Tanoue, 2008; Sabbaghzadeh et al., 2024). Its removal occurs mainly via photobleaching and microbial degradation (Stedmon and Nelson, 2015). Due to its ability to absorb ultraviolet radiation, CDOM is involved in photochemical reactions to be degraded into smaller and more bioavailable dissolved organic matter (DOM) (Kieber et al., 1989). Subsequently, this bioavailable DOM can be readily utilized by microbes, which facilitates its

remineralization (Miller and Zepp, 1995).

As the widest continental shelf region in the Western Pacific, the SCS is crucial in climate change and ocean carbon cycling. DOM flux is crucial in this region, and land-derived DOC and CDOM inputs from the Pearl River Delta into the SCS are estimated to be 3.62 × 105 t/yr and 4.93 × 10^{11} m^2/yr, respectively (Li et al., 2019). The CDOM and fluorescent DOM (FDOM) transported from the SCS through the Luzon Strait to the Western Pacific are approximately 1.13 × 10^{13} m^2/yr and 5.72 × 10^{11} RU m^3/yr, respectively (Wang et al., 2017). The relative content of CDOM in the northeastern part of the SCS fluctuates from the nearshore to the open ocean, with multiple peaks and troughs observed from the surface to deep layers (Li et al., 2022). Various processes in the northern SCS influence and regulate the sources, distribution, and transformation of DOM. The input of land-derived CDOM is critical in coastal areas, while marine biological activity is the primary source of CDOM in the open ocean (Li et al., 2019; Li et al., 2022; Wang et al., 2017; Yang et al., 2020). Photochemical processes are crucial in shaping the dynamics of DOM in the northern SCS, with humic-like components being more prone to photobleaching than protein-like components (Li et al., 2022; Yang et al., 2020). Additionally, processes such as the intrusion of the Kuroshio Current and mesoscale eddies regulate the regional distribution and behavior of CDOM (Wang et al., 2017; Zhang et al., 2020).

The nepheloid layer refers to a water layer with relatively high particle content (Eittreim et al., 1969), and the benthic nepheloid layer may be a major channel for particulate organic carbon (POC) and DOC transport from the continental shelf to the open ocean (Anderson et al., 1994; Guo et al., 1996). Extensive nepheloid layers are developed on the northern shelf of the SCS, with horizontal extensions up to several tens of kilometers (Geng et al., 2018; Zhang et al., 2014). It is estimated that the cross-shelf POC flux along the benthic nepheloid layer in the northern shelf of the SCS ranges from 3.5 ± 0.5 to 20 ± 2 mmol/m^2/d, which is approximately 0.8 to 4.7 times greater than the vertical POC flux in the basin (Cai et al., 2015; Shen et al., 2020). During the process of transport, POC is susceptible to consumption within multilevel food webs and is subsequently excreted as DOC (Steinberg and Landry, 2017). Moreover, the microbial carbon pump (MCP) is crucial in the direct degradation of POC or the conversion of DOC into refractory dissolved organic matter (RDOC) (Jiao et al., 2018). The carbon stock in the nepheloid layer is greater than that in typical water bodies (Guo and Santschi, 2000; Sempéré et al., 1994), and the distribution of CDOM in the deep layers of the northern SCS is related to the resuspension of sediments (Li et al., 2022).

However, the direct relationship between the nepheloid layer and DOM remains unclear. Suspended sediment particles in the nepheloid layer can influence POC concentrations in the water column, and the exposure of suspended sediment particles to oxidative conditions can facilitate the remineralization process of particulate organic matter (Burdige, 2007; Hartnett et al., 1998). Resuspended sediment contributed an average of 72 ± 20% to aged POC in the Japan Sea (Seo et al., 2023), and the benthic nepheloid layer may be a major pathway for transporting POC and DOC from the continental shelf to the open ocean (Anderson et al., 1994; Guo et al., 1996), which is important in regional carbon cycling. The vertical transport flux of POC from the euphotic layer to deep water was estimated at 26 ± 1 mmol/m^2/d in the cross-shelf section of the northern SCS, while the cross-shelf transport flux of POC along the benthic nepheloid layer ranged from 3.5 ± 0.5 to 20 ± 2 mmol/m^2/d. Moreover, the POC transported across the continental shelf may reach deep water, increasing the long-term carbon storage in the SCS (Hong et al., 2021).

Characterized by the diverse distribution and dynamic behavior of DOM, the SCS is renowned for its rich marine phenomena. To acquire a more comprehensive understanding of the role and mechanisms of DOM in the carbon cycle within this region, we focused on the utilization of UV-visible absorption spectra and three-dimensional fluorescence spectra of FDOM. We aimed to investigate the spatiotemporal distribution characteristics of DOC and FDOM in the northern SCS while analyzing the large impact of major physicochemical factors on the behavior of DOC and FDOM. Furthermore, we sought to explore the correlation between the distribution of nepheloid layers and the presence of DOM, to enhance our knowledge and understanding of the biogeochemical processes associated with DOM in the SCS. Our findings will contribute to a clearer understanding and improved insights into the function and mechanisms of marine nepheloid layers in the organic carbon cycle.

2. Material and methods

2.1 Study area and sampling sites

The study area in the northern SCS was investigated aboard the research vessel *Dongfanghong 3* in September 2022 as part of the National Natural Science Foundation's collaborative expedition in the northeastern South China Sea and the Luzon Strait. Two major sections, labeled B and C, were established, as illustrated in (Figure 1). Section B, encompassing stations A1 and B4–B9, covered a deep-sea basin close to the west Dongsha Islands and extended southwestward to the waters off Taiwan. It consisted of six stations arranged along the 21°N direction. Section C was located in the south of the Dongsha Islands to the north of the Zhongsha Islands, with five stations arranged along the 115°E direction. Station B8 served as a 24-hour continuous sampling site, with sampling conducted from 18:00 on September

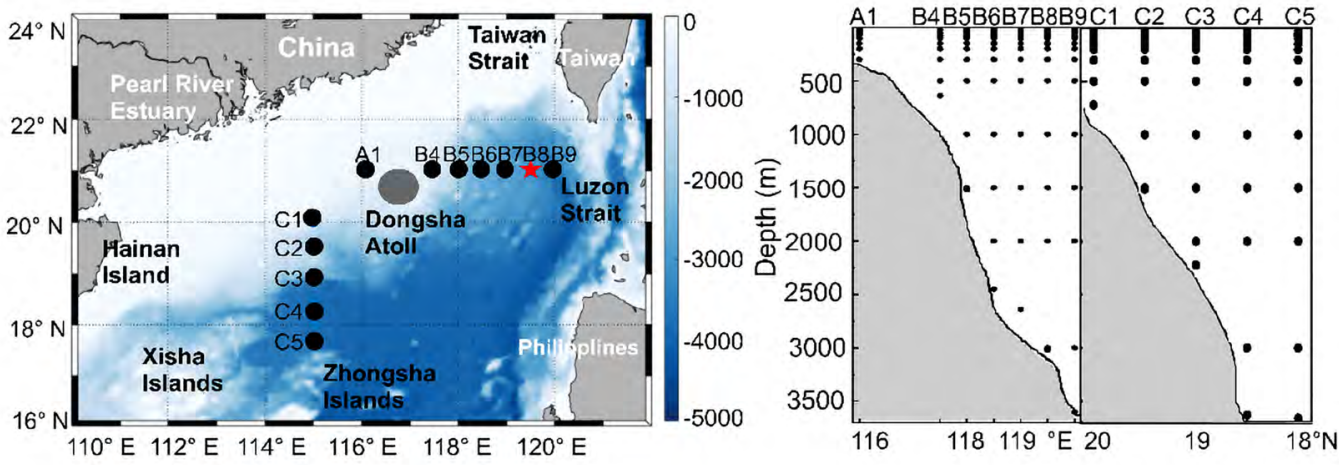

Figure 1. Study area and sampling locations in the northeastern South China Sea in September 2022.

7th to 18:00 on September 8th. Samples were collected at 3-hour intervals during this period.

2.2 Sample collection and pretreatment

Water samples were collected at various depths to investigate the water column characteristics. The sampling depths included 5 m, 25 m, 50 m, and 75 m; the deep chlorophyll maximum (DCM) layer – 100 m, 150 m, 200 m, 300 m, and 500 m; and additional layers below 500 m with intervals of 500 m, including the bottom layer. Furthermore, measurements of seawater temperature (T), salinity (S), beam attenuation (BA), dissolved oxygen (DO), and chlorophyll fluorescence, among other parameters, were conducted using a ship-mounted CTD instrument (Seabird 911 Plus, USA). The quantified water samples were filtered through 47 mm glass fiber filters (Whatman GF/F, combusted at 450°C for 4 hours) and distributed into 100 mL amber glass bottles. These samples were then frozen for subsequent analysis of dissolved nutrients, DOC, and FDOM (Xie et al., 2023).

2.3 Analysis methods

2.3.1 Dissolved organic carbon

DOC measurements were performed using the high-temperature catalytic oxidation method. A Shimadzu TOC-L Total Organic Carbon Analyzer equipped with an ASI-L automatic sampler was used to quantify DOC concentrations at the Ocean University of China. Quality control was ensured through the use of internationally standardized deep-sea water samples. The acidified samples were tested in triplicate, resulting in an analytical error of ±3% and an analytical precision below 4%.

2.3.2 Dissolved inorganic nitrogen and phosphate

Dissolved nitrate ($NO3^-$-N), nitrite ($NO2^-$-N), ammonia ($NH4^+$-N) and phosphate (DIP) were measured by spectrophotometry via a continuous flow analyzer (AutoAnalyzer 3 HR, SEAL Analytical) at the Ocean University of China. The detection limits were 0.02, 0.003, 0.03 and 0.02 μmol/L, and the maximum relative errors were 0.6%, 0.6%, 0.7% and 4.3%, respectively. The concentration of dissolved inorganic nitrogen (DIN) was the sum of $NO3^-$-N, $NO2^-$-N and $NH4^+$-N.

2.3.3 UV-visible spectroscopy analysis

The analysis of the CDOM absorption spectra was conducted using a spectrophotometer (UV-2550, Shimadzu, Japan) at the Ocean University of China. Milli-Q water served as the reference, and water samples were scanned in quartz cuvettes with a path length of 5 cm, ranging from 190 to 800 nm. The absorbance values were recorded at 1 nm intervals. The absorbance at each wavelength was corrected by subtracting the absorbance at 700 nm to account for refractive index differences between seawater and the reference Milli-Q water and to correct for baseline drift caused by the scattering of fine particles in the water sample (Del Castillo et al., 1999). This correction aimed to refine and calibrate the absorbance values.

2.3.4 Fluorescence Spectral Analysis

The excitation-emission matrix (EEM) fluorescence spectrum of the FDOM was scanned by a fluorescence spectrophotometer (F-4600, Hitachi, Japan) at the Ocean University of China. Water samples were placed in a 1 cm quartz four-way fluorescence cuvette for three-dimensional fluorescence scanning. A xenon arc lamp (450 W) was used as the excitation light source, with a selected PMT voltage

Table 1. Maximum excitation/emission wavelengths of each fluorescence component in the northern South China Sea.

Component (region)	Excitation maximum	Emission maximum	Type of fluorescent component	Peak type	Reference
C1	246	305	PheL	T	Coble (1996), Jørgensen et al. (2011)
C2	264	295	TyrL	B	Coble (1996)
C3	<240(276)	340	TrpL-1	T	Coble (1996)
C4	<240(292)	340	TrpL-2	T	Coble (1996)
C5	<240	430	HumL	A	Coble (1996)

of 700 V. Fluorescence measurements were obtained using scanning excitation spectra (Ex) from 200 to 450 nm at 2 nm intervals and emission wavelengths (Em) from 240 to 680 nm at 5 nm intervals. The scanning speed was 12000 nm/min, and the response time was 0.05 s.

Samples were diluted if the a(350) at a 1 cm path length was greater than 0.02 m^{-1} to prevent inner-filter effects (Kowalczuk et al., 2009). The sample EEMs were subtracted by Milli-Q water blank EEMs to eliminate Raman peaks, and then the excised data were replaced with interpolated data using the Delaunay triangulation method (Zepp et al., 2004). Subsequently, the EEM spectra were normalized with respect to the area under the Raman scatter peak (Ex: 350 nm) (Lawaetz and Stedmon, 2009), and the result was reported in RU. The relevant parameters of the UV-visible spectrum and EEM fluorescence spectrum are shown in Table 1.

2.3.5 Parallel factor analysis (PARAFAC) of EEM spectra

Using the DOMFluor toolbox in MATLAB R2022b software, we conducted parallel factor analysis (PARAFAC) on the acquired three-dimensional fluorescence spectral data. The study area encompassed a total of 249 excitation-emission matrices (EEMs), each matrix comprising 89 excitation bands and 106 emission bands. These EEM matrices were divided into six random subsets, with three subsets utilized for modeling and the remaining three for model validation. Each subset of EEMs was subjected to consecutive verification for models with three to six components. Three sets of data were excluded from the northern SCS samples based on the Q test for leverages, considering them outliers (section B, station B9 at 2000 m; section C, station C5 at 150 m; continuous station B8, 18:00 at 200 m). Through cross-validation, random initialization analysis, and residual analysis (Christensen et al., 2005; Olivieri, 2005), five fluorescence component models were established for the northern SCS region's water data.

Component identification was performed by matching spectra against the OpenFluor online spectral library (https://openfluor.lablicate.com/) (Murphy et al., 2014). Subsequent analysis of the identified components was then carried out. Spectral similarity was confirmed with a Tucker congruence value of 0.95 for both the excitation and emission spectra (Stedmon and Bro, 2008). Information on the identified fluorescence components in the northern SCS region is detailed in Table 1. To characterize the concentration and fluorescence intensity of each fluorescence component, the maximum fluorescence intensity (Fmax) for each component was measured in Raman units (RU) (Stedmon and Markager, 2005). The 3D-EEM results for the fluorescence components in the northern SCS are presented in Figure A.1.

2.4 Statistical analysis and calculations

Distribution maps of the research site locations were constructed using MATLAB 2022b and Surfer 23. Analysis of variance (ANOVA) was conducted utilizing IBM SPSS Statistics 26 software. Correlation analysis was performed with the aid of Origin 2023b. Cross-sectional and continuous station distribution maps for parameters were meticulously designed using Surfer 23. Canonical correlation analysis (CCA) was performed with CANOCO 5.

Optical parameters of absorption coefficient a(350) and spectral slope over $275-295$ nm ($S_{(275-295)}$).

$$a(350) = 2.303 \times \frac{A_{350}}{L} \tag{1}$$

where A_{350} and L represent the absorbance at 350 nm and the optical path length (m) (Yamashita and Tanoue, 2008).

$S_{(275-295)}$ was derived from the nonlinear fitting of the exponential decay model.

$$a(\lambda) = a(\lambda_0) \times \exp\left[-S_{(275-295)} \times (\lambda - \lambda_0)\right] \tag{2}$$

where $\lambda_0 = 285$ nm is the reference wavelength, and λ ranges from 275 to 295 nm (Helms et al., 2008).

Fluorescence index (FI) is the ratio of fluorescence intensity at emission wavelengths of 470 nm and 520 nm when excited at a wavelength of 370 nm, which characterizes the source of FDOM. FI > 1.9 indicates a microbial source predominance, and FI < 1.4 indicates a terrestrial input predominance (McKnight et al., 2001).

$$FI = \frac{I_{em,470\ nm}}{I_{em,520\ nm}}, \qquad Ex = 370\ nm \tag{3}$$

Autochthonous index (BIX) is the ratio of fluorescence intensity at emission wavelengths of 380 nm and 430 nm when excited at a wavelength of 310 nm, which reflects the relative contribution of endogenous components to FDOM. A BIX range of 0.6 to 0.7 indicates a low contribution of autochthonous components, while that of 0.7 to 0.8 suggests a moderate degree of recent autochthonous characteristics, and that of 0.8 to 1.0 indicates a strong autochthonous signature, and then that of > 1.0 suggests biological and bacterial activity or degradation (Cory and Mcknight, 2005; Huguet et al., 2009).

$$\mathrm{BIX} = \frac{\mathrm{I}_{\mathrm{em,380\ nm}}}{\mathrm{I}_{\mathrm{em,430\ nm}}}, \qquad \mathrm{Ex} = 310\ \mathrm{nm} \tag{4}$$

Humification index (HIX) is the ratio of the integrated fluorescence intensity at emission wavelengths within the ranges of $435-480$ nm and $300-345$ nm when excited at a wavelength of 254 nm, which reflects the degree of organic matter humification. The HIX < 4 indicates a relatively weak degree of DOM humification (Huguet et al., 2009).

$$\mathrm{HIX} = \frac{\sum_{345}^{480} I_\lambda}{\sum_{300}^{345} I_\lambda}, \qquad \mathrm{Ex} = 254\ \mathrm{nm} \tag{5}$$

where $\mathrm{I_{em}}$ denotes emission intensity and Ex denotes excitation wavelength.

3. Results

3.1 Distributions of physicochemical parameters and chlorophyll *a*

The distributions of major physicochemical parameters and Chl-*a* concentrations in section B of the northern SCS are illustrated in Figure 2. T exhibited a significant stratified distribution, decreasing gradually from the surface at 30°C to approximately 2.3°C in the deeper layers, with the most rapid temperature change occurring between 50 and 500 m. S ranged from 33.3 to 34.7, presenting an overall stratified distribution with lower values in the surface layer and higher values in the deeper layers. Between 100 to 250 m in section B and 50 to 200 m in section C, the salinity increased, decreased gradually toward the surface and reached the lowest values at approximately 500 m before gradually increasing again toward the bottom layer. The DO concentration in seawater followed a similar stratified pattern to that of temperature and salinity, with the highest values reaching 6.54 mg/L in the surface layer. The lowest DO concentrations occurred between 600 and 1000 m in section B and near 700 m in section C, reaching a minimum of 4.86 mg/L and gradually increasing in deeper layers.

The concentrations of DIN and DIP in seawater generally decreased in the surface layer but gradually increased in the deeper layers ($\mathrm{DIN_{max}} = 43.5\ \mu$mol/L, $\mathrm{DIP_{max}} = 2.8\ \mu$mol/L), with a distinct high-low alternation at approximately 500 m in the deeper layers. The distributions of DIN and DIP in the deep layers of section C were somewhat similar, while in section B, the DIN concentration was greater in the east and lower in the west, and DIP exhibited more pronounced high-low alternation in the horizontal direction. High concentrations of Chl-*a* were concentrated in the euphotic layer between 50 and 100 m, ranging from approximately 0.05 to 0.94 μg/L. Below the euphotic layer to the deeper layers, the Chl-*a* concentrations were significantly lower, reaching a minimum of approximately 0.01 μg/L.

The distributions of major physicochemical parameters and Chl-*a* concentrations at 24-hour anchor station B8 are depicted in Figure 3. The overall distribution of each parameter was similar to that of the cross-sectional pattern. T, S, DO, Chl-*a*, DIN and DIP concentrations all exhibited a stratified distribution from the surface to the bottom. Notably, the T, S, DO and Chl-*a* concentrations exhibited significant stratified distributions, while the DIN and DIP concentrations exhibited vertically consistent patterns below 1000 m. At 200 m, the DIN and DIP concentrations decreased from approximately 24:00 to 3:00 and near 18:00 on the second day, resembling the surface values. In the deeper layers (500 m and below), the DIN and DIP concentrations underwent significant temporal variations, with different trends between the two. The stratified distribution of the Chl-*a* concentration and its primary variation occurred within the upper 100 m, reaching a maximum of 0.25 μg/L, while below 150 m, the Chl-*a* concentration decreased to below 0.04 μg/L.

3.2 Distribution characteristics of the dissolved organic carbon concentration

The DOC concentration across the water column of the northern SCS (sections B and C) is illustrated in Figure 4. At some stations, the surface/subsurface DOC concentrations were relatively high, ranging from 0.48 to 1.81 mg/L in the upper 100 m and decreasing to 0.30 to 0.61 mg/L (average of 0.46 mg/L) below 2000 m, showing an overall decreasing trend from the surface to the deeper layers. The surface DOC concentration in section B was greater in the east and lower in the west, while in the deeper layers, it was greater in the west and lower in the east. Most stations exhibited two distinct peaks in the vertical variation in DOC concentration, one near the surface or subsurface and the other at a depth of approximately 200 m. The average DOC concentration in section C was lower than that in section B. In the vertical direction within the upper 300 m, the DOC concentration in section C showed complex variations, contrasting with that in section B. This result was generally consistent with other investigations

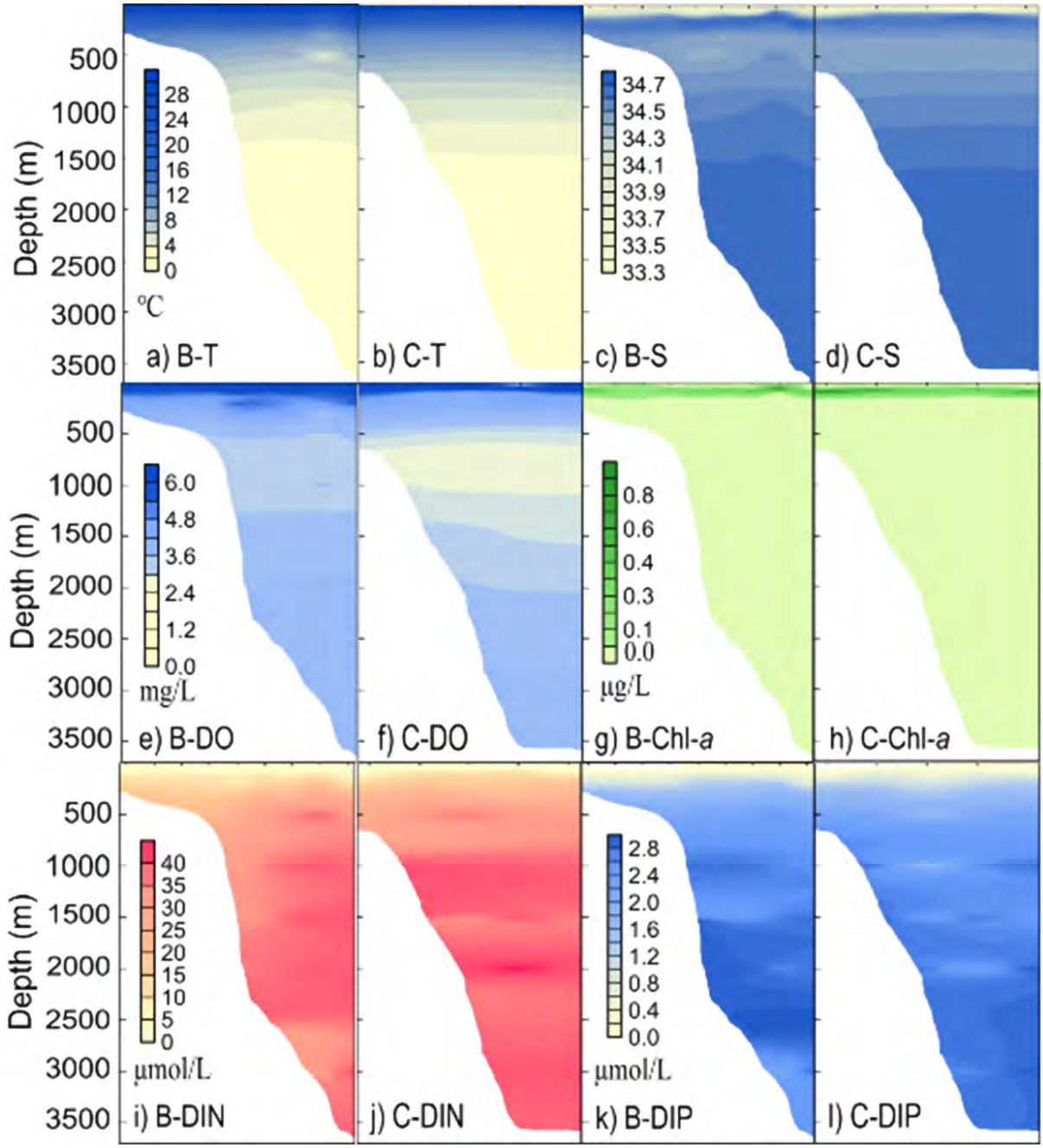

Figure 2. Study area and sampling locations in the northeastern South China Sea in September 2022.

in the northern SCS (Wu et al., 2015). There were no significant differences in DOC concentration below 2000 m among stations (ANOVA, $n = 18$, $p > 0.05$), indicating a relatively uniform distribution of deep-sea DOC in the SCS basin, possibly influenced by the rapid replenishment of water from the western Philippine Sea (Qu et al., 2000; Wu et al., 2015).

The continuous variation in DOC concentration at station B8 is depicted in Figure 4, exhibiting an overall decreasing trend from the surface layer to the bottom layer. In the upper 300 m, the horizontal distribution was relatively consistent, while in the deeper waters below 300 m, although the DOC concentration was lower, the variations in both the horizontal and vertical directions were more noticeable. Higher values were observed between 25 and 75 m from 18:00 to 03:00, after which they extended to 75–200 m. Additionally, minor increases in deep layers were observed at 9:00 and 12:00, ranging from 0.04 to 0.29 mg/L.

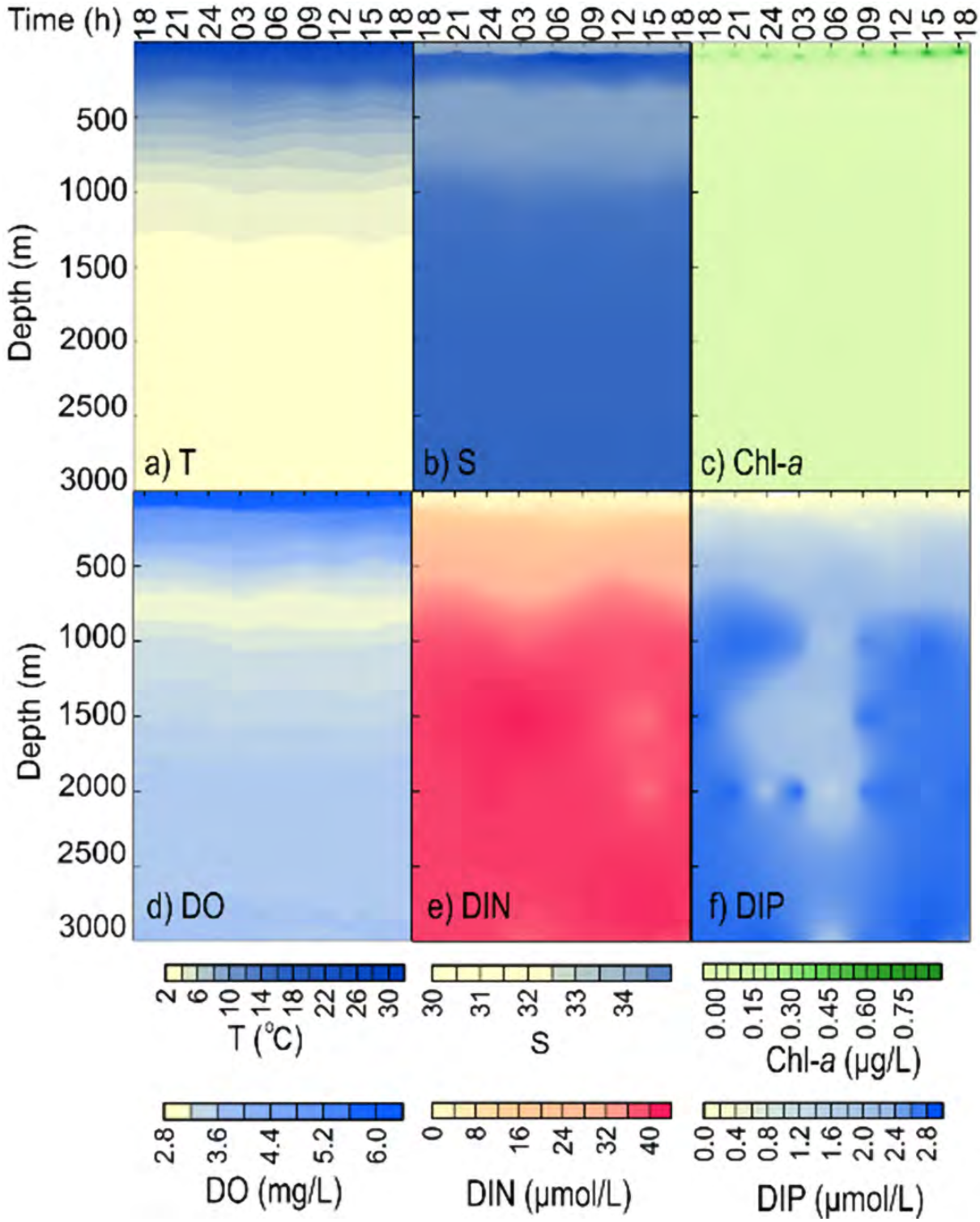

Figure 3. Study area and sampling locations in the northeastern South China Sea in September 2022.

3.3 Fluorescence spectral characteristics of DOM

Using the EEin seawater PARAFAC model, five fluorescence components were identified in the study area, including four protein-like components (C1, C2, C3 and C4) and one humic-like component (C5), as shown in Figure A.1. The maximum excitation/emission wavelengths for each fluorescence component are provided in Table 1, where C1 corresponds to phenylalanine-like fluorescence (Jørgensen et al., 2011; Wang et al., 2017), C2 corresponds to tyrosine peak B (Coble, 1996), and C3 and C4 correspond to

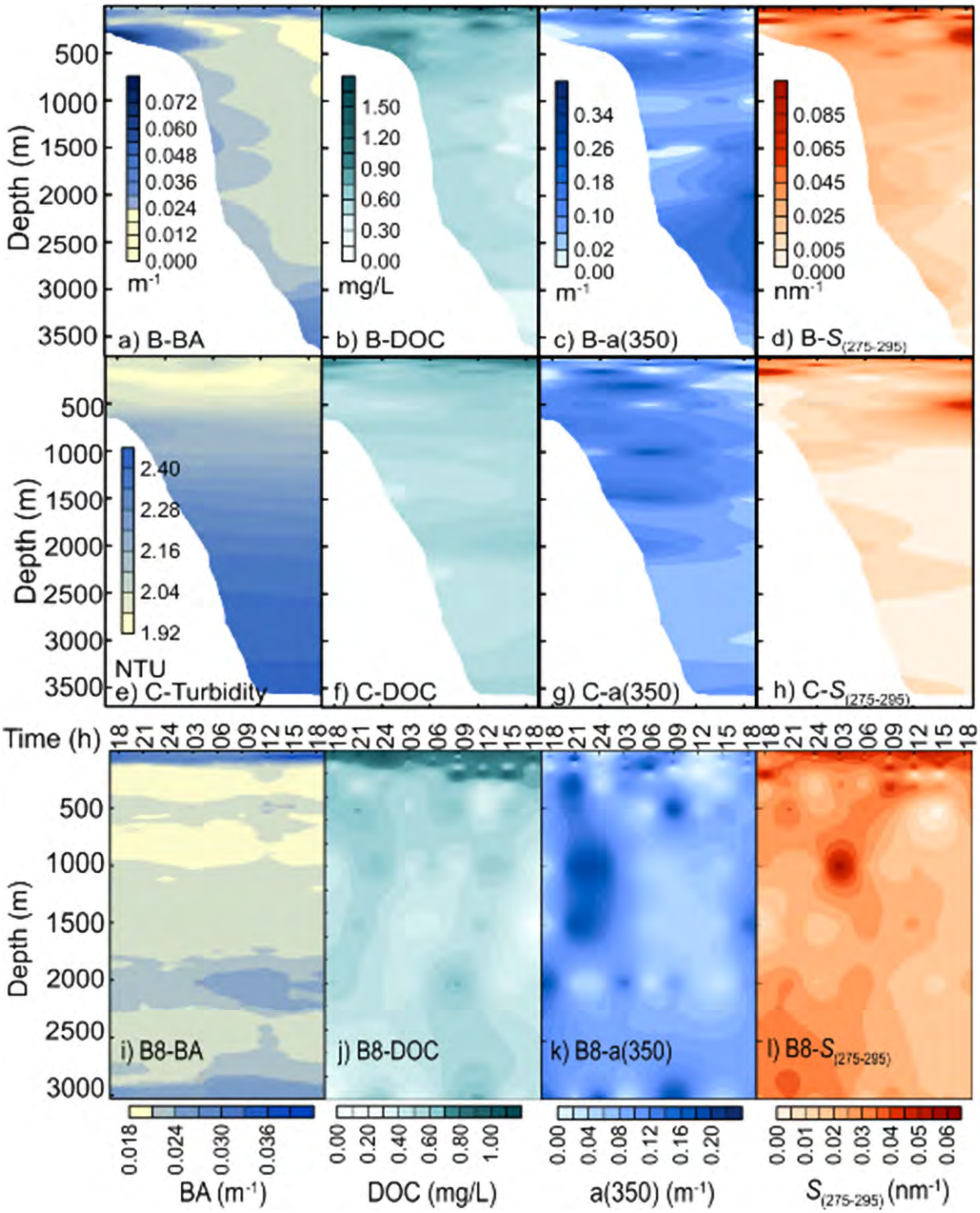

Figure 4. Study area and sampling locations in the northeastern South China Sea in September 2022

tryptophan-like fluorescence. C5 represents terrestrial humic-like fluorescence peak A (Coble, 1996), which is widely present in seawater (Jørgensen et al., 2011; Yamashita et al., 2010). When combined with the same protein, the fluorescence of tryptophan can be quenched by tyrosine, and the fluorescence of tyrosine can be quenched by phenylalanine (Lakowicz, 2006). In the northern SCS, fluorescence signals of tryptophan, tyrosine, and phenylalanine were concurrently identified, which was consistent with studies in upwelling regions such as the SCS, North Atlantic, and eastern South Pacific (Jørgensen et al., 2011; Wang et al., 2017).

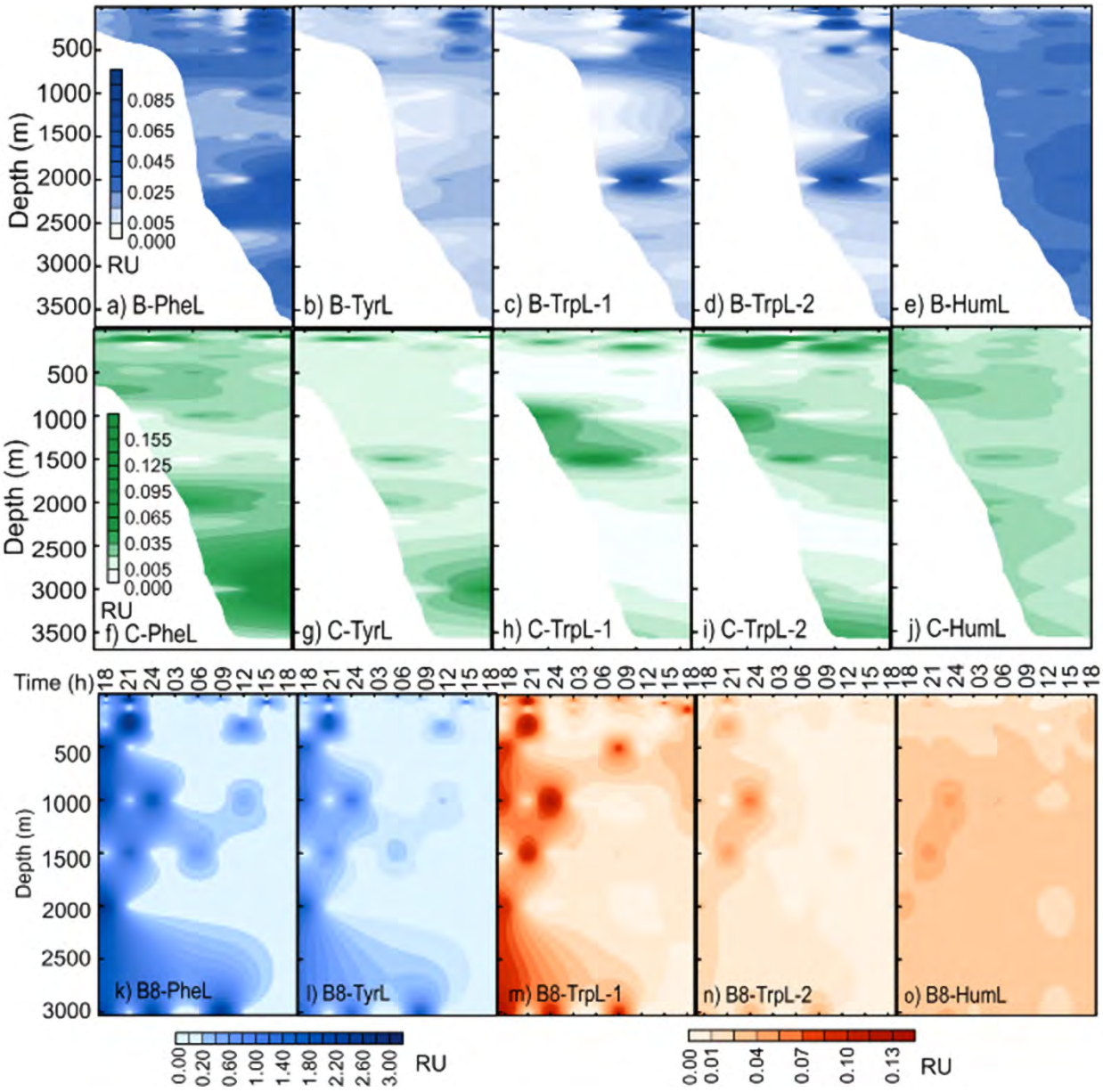

Figure 5. Study area and sampling locations in the northeastern South China Sea in September 2022.

The fluorescence intensities of the five fluorescence components across sections B and C are depicted in Figure 5. The distribution of fluorescence intensity for each component in section B was similar, generally showing lower values in the west and higher values in the east, with elevated concentrations observed at 700–800 m, 2300–2500 m, and 3000–3500 m. On average, the relative contribution of fluorescence intensity for section B followed the order of C1, C5, C3, C2 and C4 from high to low. In other words, protein-like component C1 was the dominant component, with a contribution ranging from 0.0–54.4% (average of 30.3%), followed by humic-like component C5, which contributed 7.8–54.5% (average of 26.2%), and tyrosine-like component C2, which contributed 0.0–34.3% (average of 14.8%). The contributions of the remaining two phenylalanine-like components, C3 and C4, were 0.0–48.2% (average of 15.4%) and 0.0–46.5% (average of 13.3%), respectively. In section C, the vertical distribution of fluorescence components was more pronounced than that in section B. The relative contribution rates for each component in section C followed the order of C1, C5, C4, C2 and C3 from high to low. Similarly, the tryptophan-like component C1 was the predominant fluorescence component, with a contribution range of 0.0–65.7% (average of 31.1%), followed by the humic-like component C5, which contributed 2.9–58.0% (average of 23.1%), and the phenylalanine-like component C3, which contributed 0.0–78.5% (average of 20.5%).

Despite differences in relative contribution size and spatial distribution, the protein-like components in sections B and C collectively accounted for more than 70% of the total fluorescence intensity, causing them to be the primary contributors to FDOM fluorescence. Among them, tryptophan-like components had the highest contribution rate (Jørgensen et al., 2011). With increasing depth, the protein-like components in sections B and C exhibited an overall decreasing trend, contrary to the trend observed for the humic-like components, which showed an increasing trend overall. This was consistent with the vertical distribution results of protein and humic-like components in the SCS during the spring of 2014 and in the northwestern Pacific Ocean (Wang et al., 2017; Yamashita et al., 2010).

The fluorescence intensities of components at station B8 are shown in Figure 5, where the fluorescence intensities of each component exhibit relatively consistent variations over time. In contrast to the sections, the average contribution rate of long-wavelength-excited humic-like component fluorescence was the lowest. The fluorescence intensities of the components were ranked C1, C5, C2, C3 and C4 from high to low, with tryptophan-like component C1 having the highest average contribution rate (37.3%), followed by humic-like component C5 (average of 22.6%), tyrosine-like component C2 (average of 18.6%), and phenylalanine-like components C3 and C4 (average of 11.1% and 10.4%, respectively). Consistent with the section results, protein-like fluorescence intensity accounted for 20.6–99.9% of the total fluorescence intensity, causing it to be the main contributor. In the upper 100 m, the protein-like fluorescence intensity was relatively high, while with increasing water depth, the humic-like fluorescence intensity gradually increased, but protein-like fluorescence remained dominant.

4. Discussion

4.1 Biological origin of FDOM

The FI and BIX results for the study area are illustrated in Figure 6. The FI values were greater in the surface layer and exhibited alternating decreased toward the deeper layers. Stations C2 and C4 in section C showed the highest FIs in the surface layer, exceeding six times that of other water bodies in the investigation area. The overall elevated FI suggested intense biological activity in the study area, indicating critical marine characteristics (McKnight et al., 2001). The trend in BIX changes was generally similar to that in FI, showing higher values in the surface layer and gradually decreasing toward the deeper layers with a degree of high-low alternation (Wang et al., 2017). Higher BIX values in the surface layer indicated that the fluorescent DOM mainly originates from in situ biological activity (Huguet et al., 2009).

The continuous FI values at station B8 were generally high, with significant spatiotemporal variations ranging from 0.6 to 6.8 (with an average of 2.4). These values exhibited an overall high-low alternation in a patchy distribution. The highest and lowest values occurred in the upper 100 m, and the changes in the FI were rapid in time and confined to a small spatial extent. The BIX values ranged from 0.51 to 3.47 (average of 1.38), with similar variations to those of the FI in the upper 200 m, which higher surface layer values gradually decreasing toward the deeper layers. The variation pattern in the deeper layers was generally opposite to that of the FI. During the period from 9:00 to 18:00, the BIX values were lower, indicating a lower contribution from autochthonous substances.

The correlation analysis between the FI, BIX, and the fluorescence intensity of protein-like and humic-like components is presented in Figure A.2. The BIX showed a significant positive correlation with protein-like fluorescence (r= 0.2653, $p < 0.001$, n= 274) and a significant negative correlation with humic-like fluorescence (r= −0.2371, $p < 0.001$, n=274). While both the FI and BIX indicated the biological origin characteristics of FDOM, the FI primarily represents contributions from bacterial and algal secretions when indicating a marine source (McKnight et al., 2001), and higher BIX values indicate in situ bacterial activity or degradation products (Huguet et al., 2009). In the study area, the BIX showed a significant positive correlation with protein-like fluorescence, suggesting that in situ bacterial activity is the primary source of protein-like components (Coble, 1996; Sierra et al., 1994). However, the BIX exhibited a significant negative correlation with both the FI and humic-like fluorescence. The high proportion of humic-like fluorescence (average of 24.2%), along with significant positive correlations with DIN (r= 0.7120, $p <$ 0.001, n= 274) and DIP (r = 0.6779, $p < 0.001$, n= 274), as products of microbial remineralization, indicated that humic-like components may be essential carbon sources supporting bacterial regeneration activities (Yamashita et al., 2010).

4.2 Influence of major physicochemical factors on DOM

The DOM characteristics were represented by the DOC concentration and FDOM absorption properties, and FDOM fluorescence components. Linear correlation analysis with major physicochemical factors such as T, S and nutrients was conducted, as shown in Figure A.2 . CCA results are presented in Figure 7. The euphotic layer depth in the study area ranges between 50 and 100 m and gradually decreases from east to west (Tang et al., 2007). Consequently, the water quality points were categorized into three classes: 0–100 m, representing the euphotic layer; 150–500 m, representing the subeuphotic layer; and 500 m, representing the deep layer. Statistical analysis revealed differences in the DOM characteristics among the euphotic layer, subeuphotic layer, and deep layer. Although the characteristics of the euphotic layer and deep layer DOM dif-

fered, the subeuphotic layer partly exhibited characteristics of both the euphotic and deep layers.

DOC showed a significant correlation with T, S, DO, nutrients and Chl-*a*. This suggested that DOC distribution is influenced by a combination of physicochemical and biological factors, including the secretion and release of phytoplankton (Chen and Wagnersky, 1993), oxidation and degradation under DO dominance (Peltzer and Hayward, 1996), and conditions related to DOC production and oxidation. The weak correlation between a(350) and DOC implied different processes and transformation mechanisms for FDOM and DOC in the study area. The crucial factors influencing FDOM are T, DO and nutrients. Simultaneous analysis of FDOM fluorescence components, such as humic-like component C5, revealed a strong negative correlation with DOC and various physicochemical and Chl-*a* factors. The direction of the correlation between these factors and C5 was opposite to that of DOC with the same factors. This indicated that changes in humic-like components are influenced by multiple factors and, as a relatively stable component in DOC, primarily arise from active components within DOC (Jiao et al., 2018). Both a(350) and C5 showed strong negative correlations with $S_{(275-295)}$, suggesting that the molecular size of FDOM was primarily regulated by humic-like FDOM components. Higher abundance of humic-like FDOM contributes to more complex FDOM molecular structures, resulting in lower $S_{(275-295)}$ (Helms et al., 2008).

Within the FDOM protein-like fluorescence components, only phenylalanine-like C1 showed a positive correlation with S, and tryptophan-like C4 showed a positive correlation with Chl-*a*. Only tryptophan-like C3 showed a significant correlation with physicochemical factors and Chl-*a*. The correlation directions of these fluorescence components with physicochemical factors were opposite to those of humic-like component C5, indicating a cross-process between protein-like and humic-like components in FDOM in the study area. The results with lower correlation coefficients or no correlation with major physicochemical factors and Chl-*a* suggested that the production and transformation of protein-like components are less directly influenced by major physicochemical factors and primary production activities, potentially being more closely associated with bacterial regeneration and degradation activities (Cammack et al., 2004).

The fluorescence intensity of humic-like components exhibited a highly significant negative correlation with DO, indicating a large influence of oxidation processes on the transformation and degradation of humic-like components. In contrast to the relationship between humic-like components and DO, tryptophan-like C3 showed a positive correlation with DO. Other protein-like components exhibited no correlation with DO, and total protein fluorescence had no correlation with DO (Figure 8h). It was hypothesized that amino acids, primarily produced by bacteria, were more active in nature, with higher production rates and faster transformation and degradation. The bacterial regeneration activities were relatively less restricted by redox conditions, resulting in a weak association between protein-like fluorescence and dissolved oxygen. The linear correlation analysis of the fluorescence intensity for the five FDOM fluorescence components in the study area is presented in Figure A.2. The fluorescence intensities of the four protein-like components C1, C2, C3 and C4 were strongly correlated. The protein-like components C1, C2, C3 and C4 were significantly correlated with the humic-like component C5, albeit with a slightly lower correlation. The above correlation analysis indicated consistency in the source and behavior of protein-like components in the FDOM of the northern SCS and a close relationship between the source and behavior of humic-like components and protein-like components. In subsequent calculations, protein-like components were grouped for analysis and discussion.

4.3 Coupling between the nepheloid layer and DOM

Extensive nepheloid layers have developed over the SCS shelf, with vertical thicknesses exceeding 100 m and horizontal extensions covering several tens of kilometers (Zhang et al., 2014; Geng et al., 2018). Observations along section B in this study (Figure 4a) indicated higher BA values in both the surface and bottom layers.

Between 500 m and 2500 m, there were five regions with elevated BAs extending horizontally from the bottom layer, with the highest BA occurring near 500 m. These horizontally distributed high BA values indicated the location, extent and concentration of particulate matter in the nepheloid layer. Continuous observations at station B8 revealed that, apart from the surface and bottom layers, BA near 500 m and 2000 m remained higher than that in the surrounding layers throughout the 24-hour observation period, indicating the persistent presence of the nepheloid layer.

The relationships between the different forms of DOM and BA in the study area are illustrated in Figure 8. Generally, DOC showed a positive correlation with BA, indicating that the nepheloid layer region likely had higher DOC concentrations. In the surface seawater, the contribution of particles to BA was mainly from phytoplankton-dominated planktonic biogenic particles. Figure 8b shows a significant positive correlation between Chl-*a* and BA in the euphotic layer (0–100 m), while Chl-*a* concentrations were low, close to the detection limit, in the subeuphotic and deep layers, exhibiting no apparent correlation with BA. Despite phytoplankton particles being the primary contributors to BA in the euphotic layer, DOC did not show a significant correlation with Chl-*a* (Figure 8c). Further analysis of FDOM components, including humic-like components and protein-like components, in relation to Chl-*a*

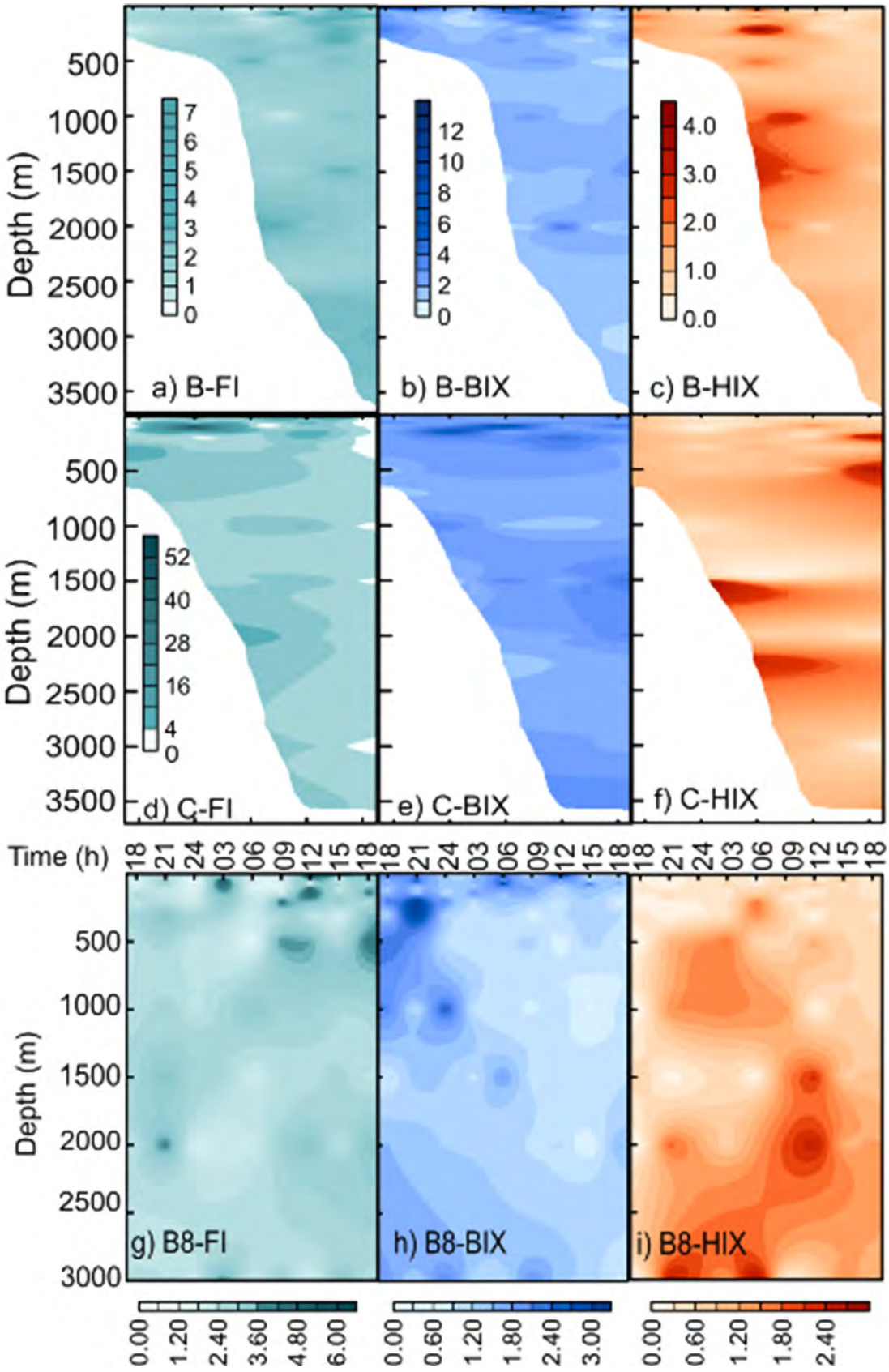

Figure 6. Study area and sampling locations in the northeastern South China Sea in September 2022.

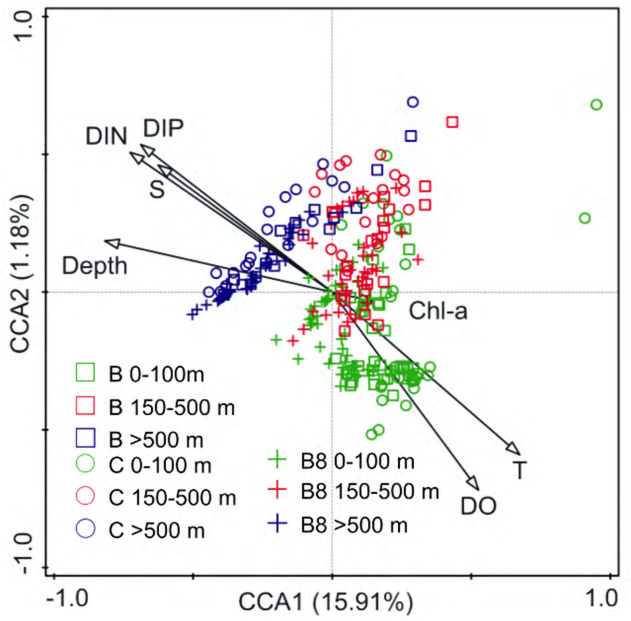

Figure 7. Study area and sampling locations in the northeastern South China Sea in September 2022.

concentrations revealed that humic-like fluorescence intensity was positively correlated with Chl-*a* (Figure 8d), while protein-like fluorescence intensity did not exhibit a clear pattern in relation to Chl-*a* (Figure 8e). Thus, it was suggested that the humic-like components in the euphotic layer water are mainly derived from the transformation of organic matter from phytoplankton, while protein-like components may originate from bacterial regeneration activities (Cammack et al., 2004; Yamashita and Tanoue, 2004).

Further analysis of the relationship between humic-like component and protein-like component fluorescence with Chl-*a* and BA revealed the following patterns: Humic-like fluorescence intensity was positively correlated with Chl-*a* Figure 8d), while protein-like fluorescence intensity did not exhibit a consistent pattern in relation to Chl-*a* concentrations (Figure 8e). In the euphotic layer, humic-like fluorescence did not show a correlation with BA, whereas in the subeuphotic and deep layers, humic-like fluorescence was positively correlated with BA (Figure 8g). On the other hand, there was no significant correlation between protein-like fluorescence and BA. Phytoplankton particles in the euphotic layer were suggested to be the primary source of humic-like components, while in the subeuphotic and deep layers, suspended particles are the carrier, becoming the main source of humic-like components. Protein-like components are mainly derived from bacterial regeneration activities (Cammack et al., 2004). Bacterial regeneration activities, influenced by environmental conditions, contribute greatly to the transformation and degradation of organic matter (Williams, 2000). We did not explicitly establish the associations between protein-like fluorescence and phytoplankton particles in the euphotic layer or between protein-like fluorescence and suspended particles in the deep layer.

5. Conclusions

The marine nepheloid layer developed under the comprehensive effects of ocean dynamics and geomorphology in the northern SCS, which largely impact the existence, transformation and migration of nutrients and organic matter (Burdige, 2007; Seo et al., 2023). BA can indicate the location and extent of the marine nepheloid layer. There are 3 patches in the higher BA that extend horizontally from the bottom to the water in section B in the SCS, in which the patch with the highest BA is near the bottom 500 m and extends eastward. Elevated DOC in the nepheloid layer coincided with higher BA, reflecting a consistent positive DOC-BA correlation from surface to bottom waters. Moreover, the fluorescence intensities of the protein-like and humic-like components of FDOM present dissimilar relationships with BA, which imply that the regulatory mechanisms of the nepheloid layer to different sources of DOC are inconsistent. The positive relationships between BA, Chl-*a* concentrations and humic-like fluorescence suggest that phytoplankton particles primarily contribute to the suspended particulate matter in the euphotic nepheloid layer (Madron et al., 2017), and humic-like components originate from the organic matter of phytoplankton (Yamashita and Tanoue, 2004; Cammack et al., 2004). BA is closely associated with DOC and humic-like components in the euphotic zone, where Chl-*a* decays to the detection limit. It was reported that suspended particles in the marine nepheloid layer provides hosting sites for microorganisms (Thiele et al., 2019), and the nonliving particles of organic carbon insufficiently support the bacterial demand (Boetius et al., 2000). Protein-like components are more active than humic-like components and are associated with regenerative bacterial activities. Generally, the marine nepheloid layer primarily influences the distributions of DOC and humic-like components, are regulated by phytoplankton particles in the euphotic zone and by nonliving and bacterial particles in the euphotic zone.

CRediT authorship contribution statement

Xiaochao Sui: Data curation and writing of the original draft. Li Zou: Conceptualization, writing-review and editing. Tian Chen and Yinuo Wang: Methodology and data curation. Chaoqi Zhu: Investigation and methodology. Yonggang Jia: Funding acquisition and project administration.

Conflict of interest

None declared.

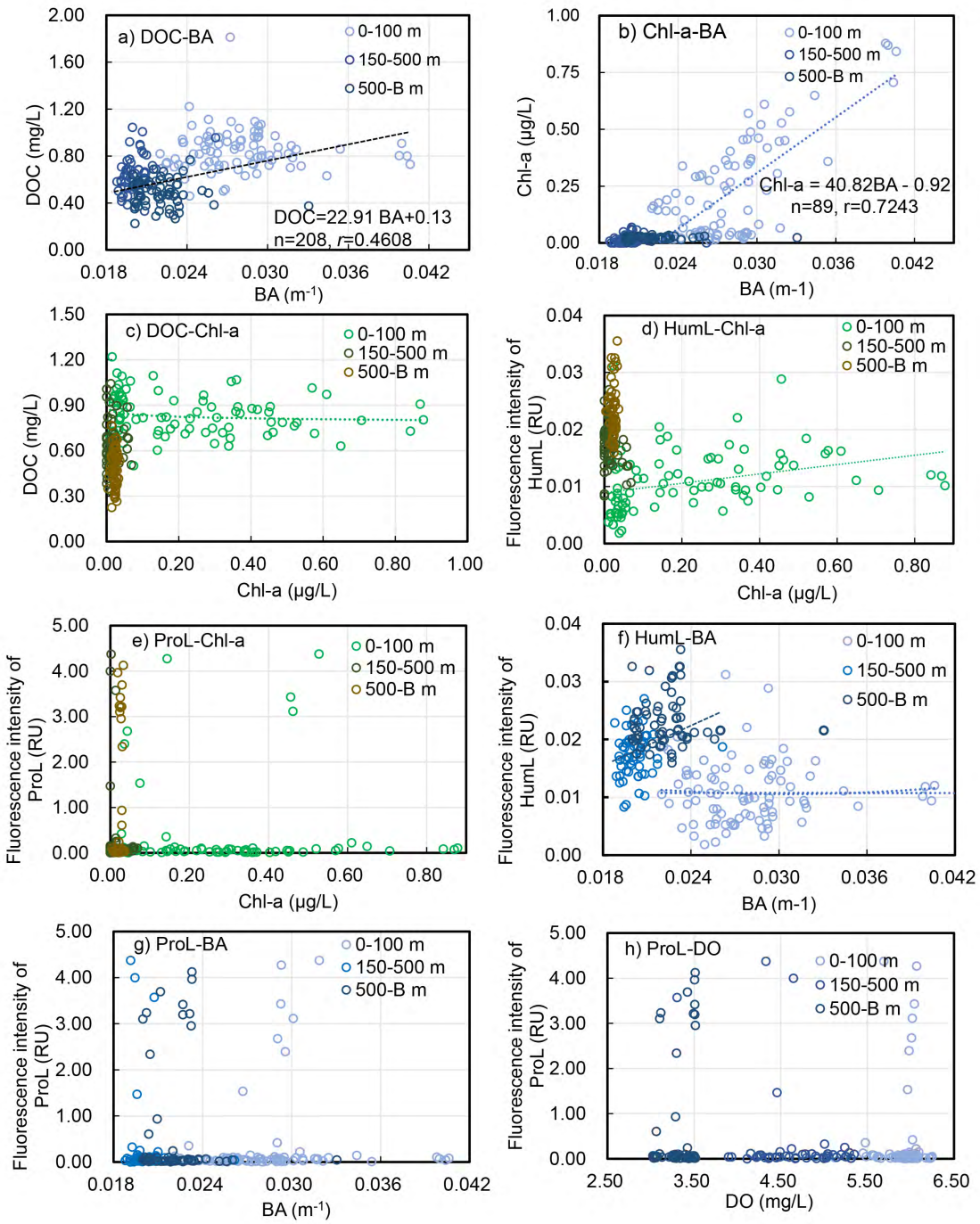

Figure 8. Study area and sampling locations in the northeastern South China Sea in September 2022.

Data availability

The data will be made available upon request.

Acknowledgments

This study is supported by the National Science Foundation of China (No. 41831280). Data and samples were collected onboard the r/v *Dongfanghong 3*, which implemented the open research cruise NORC2022-05 supported by the NSFC Shiptime Sharing Project (project number: 42149905).

Appendix A. Supplementary materials

Supplementary data associated with this article can be found online. Please follow this link to see the supplementary data associated with this article.

References

Anderson, R.F., Rowe, G.T., Kemp, P.F., Trumbores, S., Biscaye, P.E., 1994. *Carbon budget for the mid-slope depocenter of the Middle Atlantic Bight*. Deep Sea Res. Pt. II 41(2–3), 669–703. https://doi.org/10.1594/PANGAEA.730406

Burdige, D.J., 2007. *Preservation of organic matter in marine sediments: controls, mechanisms, and an imbalance in sediment organic carbon budgets*. Chem. Rev. 107(2), 467–485. https://doi.org/10.1021/cr050347q

Boetius, A., Springer, B., Petry, C., 2000. *Microbial activity and particulate matter in the benthic nepheloid layer (BNL) of the deep Arabian Sea*. Deep Sea Res. Pt. II 47(14), 2687–2706. https://doi.org/10.1016/S0967-0645(00)00045-X

Cai, P., Zhao, D., Wang, L., Huang, B., Dai, M., 2015. *Role of particle stock and phytoplankton community structure in regulating particulate organic carbon export in a large marginal sea*. J. Geophys. Res-Oceans 120(3), 2063-2095. https://doi.org/10.1002/2014JC010432

Cammack, W.L., Kalff, J., Prairie, Y.T., Smith, E.M., 2004. *Fluorescent dissolved organic matter in lakes: relationships with heterotrophic metabolism*. Limnol. Oceanogr. 49(6), 2034–2045. https://doi.org/10.4319/lo.2004.49.6.2034

Chen, W., Wagnersky, P.J., 1993. *High-temperature combustion analysis of dissolved organic carbon produced in phytoplankton cultures*. Mar. Chem. 41(1–3), 167–171. https://doi.org/10.1016/0304-4203(93)90115-5

Christensen, J.H., Hansen, A.B., Mortensen, J., Andersen, O., 2005. *Characterization and matching of oil samples using fluorescence spectroscopy and parallel factor analysis*. Anal. Chem. 77(7), 2210–2217. https://doi.org/10.1021/ac048213k

Coble, P.G., 1996. *Characterization of marine and terrestrial DOM in seawater using excitation-emission matrix spectroscopy*. Mar. Chem. 51(4), 325–346. https://doi.org/10.1016/0304-4203(95)00062-3

Del Castillo, C.E., Coble, P.G., Morell, J.M., Lopez, J.M., Corredor, J.E., 1999. *Analysis of the optical properties of the Orinoco River plume by absorption and fluorescence spectroscopy*. Mar. Chem. 66(1–2), 35–51. https://doi.org/10.1016/s0304-4203(99)00023-7

Eittreim, S., Ewing, M., Thorndike, E.M., 1969. *Suspended matter along the continental margin of the North American Basin*. Deep-Sea Res. Oceanogr. Abstr. 6(6), 613–624. https://doi.org/10.1016/0011-7471(69)90062-x

Friedlingstein, P., O'Sullivan, M., Jones, M. W., Andrew, R. M., Gregor, L., Hauck, J., Le Quéré, C., Luijkx, I. T., Olsen, A., Peters, G. P., Peters, W., Pongratz, J., Schwingshackl, C., Sitch, S., Canadell, J. G., Ciais, P., Jackson, R. B., Alin, S. R., Zheng, B., 2022. *Global Carbon Budget 2022*. Earth System Sci. Data 14(11), 4811–4900. https://doi.org/10.5194/essd-14-4811-2022

Geng, M., Song, H., Guan, Y., Chen, J., 2018. *Research on the distribution and characteristics of the nepheloid layers in the northern South China Sea by use of seismic oceanography method*. Chin. J. Geophys. 61(02), 636–648. https://doi.org/10.6038/cjg2018L0662

Guo, L., Santschi, P.H., 2000. *Sedimentary sources of old high molecular weight dissolved organic carbon from the ocean margin benthic nepheloid layer*. Geochim. Cosmochim. Acta, 64(4), 651–660. https://doi.org/10.1016/s0016-7037(99)00335-x

Guo, L., Santschi, P.H., Cifuentes, L.A., Trumbore, S.E., Southon, J., 1996. *Cycling of high-molecular-weight dissolved organic matter in the Middle Atlantic Bight as revealed by carbon isotopic (13C and 14C) signatures*. Limnol. Oceanogr. 41(6), 1242–1252. https://doi.org/10.4319/lo.1996.41.6.1242

Hansell, D.A., Carlson, C.A., 1998. *Deep ocean gradients in dissolved organic carbon concentrations*. Nature 395(6699), 263–266. https://doi.org/10.1038/26200

Hansell, D. A., Carlson, C. A., Repeta, D. J., Schlitzer, R., 2012. *Dissolved organic matter in the ocean: A controversy stimulates new insights*. Nature Geosci. 5(12), 848–854. https://doi.org/10.5670/oceanog.2009.109

Hartnett, H.E., Keil, R.G., Hedges, J.I., Devol, A.H., 1998. *Influence of oxygen exposure time on organic carbon preservation in continental margin sediments*. Nature 391(6667), 572–575. https://doi.org/10.1038/35351

Helms, J.R., Stubbins, A., Ritchie, J.D., Minor, E.C., Kieber, D.J., Mopper, K., 2008. *Absorption spectral slopes and slope ratios as indicators of molecular weight, source, and photobleaching of chromophoric dissolved organic matter*. Limnol. Oceanogr. 53(3), 955–969. https://doi.org/10.4319/lo.2008.53.3.0955

Hong, Q., Peng, S., Zhao, D., Cai, P., 2021. *Cross-shelf export of particulate organic carbon in the northern South China Sea: Insights from a 234Th mass balance*. Prog. Oceanogr. 193, 102532. https://doi.org/10.1016/j.pocean.2021.102532

Huguet, A., Vacher, L., Relexans, S., Saubusse, S., Froidefond, J.M., Parlanti, E., 2009. *Properties of fluorescent dissolved organic matter in the Gironde Estuary*. Org. Geochem. 40(6), 706–719. https://doi.org/10.1016/j.orggeochem.2009.03.002

Jiao, N., Cai, R., Zheng, Q., Tang, K., Liu, J., Jiao, F., Wallace, D., Chen, F., Li, C., Amann, R., Benner, R., Azam, F., 2018. *Unveiling the enigma of refractory carbon in the ocean*. Natl. Sci. Rev. 5(4), 459–463. https://doi.org/10.1093/nsr/nwy020

Jørgensen, L., Stedmon, C.A., Kragh, T., Markager, S., Middelboe, M., Søndergaard, M., 2011. *Global trends in the fluorescence characteristics and distribution of marine dissolved organic matter*. Mar. Chem. 126(1–4), 139–148. https://doi.org/10.1016/j.marchem.2011.05.002

Kieber, D., McDaniel, J., Mopper, K., 1989. *Photochemical source of biological substrates in seawater: implications for carbon cycling*. Nature 341(6243), 60–62. https://doi.org/10.1038/341637a0

Kowalczuk, P., Durako, M.J., Young, H., Kahn, A.E., Cooper, W.J., Gonsior, M., 2009. *Characterization of dissolved organic matter fluorescence in the South Atlantic Bight with the use of PARAFAC model: Interannual variability*. Mar. Chem. 113(3–4), 182–196. https://doi.org/10.1016/j.marchem.2009.01.015

Lakowicz, J.R., 2006. *Principles of Fluorescence Spectroscopy*, 3 edn., Springer-Verlag US, 954 pp. https://doi.org/10.1007/978-0-387-46312-4

Lawaetz, A.J., Stedmon, C.A., 2009. *Fluorescence intensity calibration using the Raman scatter peak of water*. Appl. Spectrosc. 63(8), 936–940. https://doi.org/10.1366/000370209788964548

Li, Y., Song, G., Massicotte, P., Yang, F., Li, R., Xie, H., 2019. *Distribution, seasonality, and fluxes of dissolved organic matter in the Pearl River (Zhujiang) estuary, China*. Biogeosciences 16(13), 2751–2770. https://doi.org/10.5194/bg-16-2751-2019

Li, Y., Zhang, Y., Li, Z., Wan, J., Dang, C., Fu, J., 2022. *Characterization of colored dissolved organic matter in the northeastern South China Sea using EEMs-PARAFAC and absorption spectroscopy*. J. Sea Res. 180, 102159.

Madron, X.D.D., Ramondenc, S., Berline, L., Houpert, L., Bosse, A., Martini, S., Guidi, L., Conan, P., Curtil, C., Delsaut, N., Kunesch, S., Ghiglione, J.F., Marsaleix, P., Pujo-Pay, M., Séverin, T., Testor, P., Tamburini, C., the ANTARES collaboration, 2017. *Deep sediment resuspension and thick nepheloid layer generation by open-ocean convection*. J. Geophys. Res. Ocean. 122(3), 2291–2318. https://doi.org/10.1002/2016JC012062

McKnight, D.M., Boyer, E.W., Westerhoff, P.K., Doran, P.T., Kulbe, T., Andersen, D.T., 2001. *Spectrofluorometric characterization of dissolved organic matter for indication of precursor organic material and aromaticity*. Limnol. Oceanogr. 46(1), 38–48. https://doi.org/10.4319/lo.2001.46.1.0038

Miller, W.L., Zepp, R.G., 1995. *Photochemical production of dissolved inorganic carbon from terrestrial organic matter: significance to the oceanic organic carbon cycle*. Geophys. Res. Lett. 22, 417–420. https://doi.org/10.1029/94GL03344

Murphy, K.R., Stedmon, C.A., Wenig, P., Bro, R., 2014. *OpenFluor–an online spectral library of auto-fluorescence by organic compounds in the environment*. Anal. Methods 6(3), 658–661. https://doi.org/10.1039/C3AY41935E

Olivieri, A.C., 2005. *Computing sensitivity and selectivity in parallel factor analysis and related multiway techniques: the need for further developments in net analyte signal theory*. Anal. Chem. 77(15), 4936–4946. https://doi.org/10.1021/ac050146m

Peltzer, E.T., Hayward, N.A., 1996. *Spatial and temporal variability of total organic carbon along 140 W in the equatorial Pacific Ocean in 1992*. Deep Sea Res. Pt. II 43(4– 6), 1155–1180. https://doi.org/10.1016/0967-0645(95)00014-3

Qu, T., Mitsudera, H., Yamagata, T., 2000. *Intrusion of the north Pacific waters into the South China Sea*. J. Geophys. Res.-Oceans 105(C3), 6415–6424. https://doi.org/10.1029/1999JC900323

Sabbaghzadeh, B., Uher, G., Upstill-Goddard, R., 2024. *Dynamics of chromophoric dissolved organic matter in the Atlantic Ocean: unravelling province dependent relationships, optical complexity, and environmental influences*. Front. Mar. Sci. 11, 1432133. https://doi.org/10.3389/fmars.2024.1432133

Sempéré, R., Cauwet, G., Randon, J., 1994. *Ultrafiltration of seawater with a zirconium and aluminum oxide tubular membrane: application to the study of colloidal organic carbon distribution in an estuarine bottom nepheloid layer*. Mar. Chem. 46(1–2), 49–60. https://doi.org/10.1016/0304-4203(94)90044-2

Seo, J., Kim, G., Seo, H., Na, T., Noh, S., Hwang, J., 2023. *Sources and behaviors of particulate organic carbon, iron, and manganese in the bottom nepheloid layer of the southwestern East Sea (Japan Sea)*. Mar. Chem. 257, 104323. https://doi.org/10.1016/j.marchem.2023.104323

Shen, J., Jiao, N., Dai, M., Wang, H., Qiu, G., Chen, J., Li, H., Kao, S.-J., Yang, J.-Y.T., Cai, P., Zhou, K., Yang, W., Zhu, Y., Liu, Z., Chen, M., Zuo, Z., Gaye, B., Wiesner, M.G., Zhang, Y., 2020. *Laterally transported particles from margins serve as a major carbon and energy source for dark ocean ecosystems*. Geophys. Res. Lett. 47(18), e2020GL088971. https://doi.org/10.1029/2020GL088971

Sierra, M.D.S., Donard, O.F.X., Lamotte, M., Belin, C., Ewald, M., 1994. *Fluorescence spectroscopy of coastal and marine waters*. Mar. Chem. 47(2), 127–144. https://doi.org/10.1016/0304-4203(94)90104-x

Stedmon, C. A., Bro, R., 2008. *Characterizing dissolved organic matter fluorescence with parallel factor analysis: a tutorial*. Limnol. Oceanogr.-Methods 6(11), 572–579. https://doi.org/10.4319/lom.2008.6.572

Stedmon, C.A., Markager, S., 2005. *Tracing the production and degradation of autochthonous fractions of dissolved organic matter by fluorescence analysis*. Limnol. Oceanogr. 50(5), 1415–1426.

https://doi.org/10.4319/lo.2005.50.5.1415

Stedmon, C.A., Nelson, N.B., 2015. *The optical properties of DOM in the ocean*. [in:] *Biogeochemistry of marine dissolved organic matter*. Acad. Press, 481–508. https://doi.org/10.1016/b978-0-12-405940-5.00010-8

Steinberg, D.K., Landry, M.R., 2017. *Zooplankton and the ocean carbon cycle*. Annu. Rev. Mar. Sci. 9(1), 413–444. https://doi.org/10.1146/annurev-marine-010814-015924

Tang, S., Chen, C., Zhan, H., Xu, D., Liu, D., 2007. *Remote sensing inversion of true optical depth in South China Sea*. J. Trop. Oceanogr. 26(1), 7. https://doi.org/10.3969/j.issn.1009-5470.2007.01.002

Thiele, S., Basse, A., Becker, J. W., Lipski, A., Iversen, M. H., Mollenhauer, G., 2019. *Microbial communities in the nepheloid layers and hypoxic zones of the Canary Current upwelling system*. MicrobiologyOpen 8(5), e00705. https://doi.org/10.1002/mbo3.705

Wang, C., Guo, W., Li, Y., Stubbins, A., Li, Y., Song, G., Wang, L., Cheng, Y., 2017. *Hydrological and biogeochemical controls on absorption and fluorescence of dissolved organic matter in the Northern South China Sea*. J. Geophys. Res.-Biogeosci. 122(12), 3405–3418. https://doi.org/10.1002/2017JG004100

Williams, P.J.L.B., 2000. *Heterotrophic bacteria and the dynamics of dissolved organic material*. Microb. Ecol. Oceans. https://api.semanticscholar.org/CorpusID:221557347

Wu, K., Dai, M., Chen, J., Meng, F., Li, X., Liu, Z., Du, C., Gan, J., 2015. *Dissolved organic carbon in the South China Sea and its exchange with the Western Pacific Ocean*. Deep Sea Res. Pt. II 122, 41–51. https://doi.org/10.1016/j.dsr2.2015.06.013

Xie, L., Guan, W., Zou, L., Xia, B., Ji, G., 2023. *Composition, variation and contribution of chromophoric dissolved organic matter in Laizhou Bay estuaries, North China*. Mar Environ Res. 190, 106102. https://doi.org/10.1016/j.marenvres.2023.106102

Yamashita, Y., Cory, R.M., Nishioka, J., Kuma, K., Tanoue, E., Jaffé, R., 2010. *Fluorescence characteristics of dissolved organic matter in the deep waters of the Okhotsk Sea and the northwestern North Pacific Ocean*. Deep Sea Res. Pt. II 57(16), 1478–1485. https://doi.org/10.1016/j.dsr2.2010.02.016

Yamashita, Y., Tanoue, E., 2004. *In situ production of chromophoric dissolved organic matter in coastal environments*. Geophys. Res. Lett. 31, L14302. https://doi.org/10.1029/2004GL019734

Yamashita, Y., Tanoue, E., 2008. *Production of bio-refractory fluorescent dissolved organic matter in the ocean interior*. Nat. Geosci. 1, 579–582. https://doi.org/10.1038/ngeo279

Yang, F., Song, G., Massicotte, P., Wei, H., Xie, H., 2020. *Depth-resolved photochemical lability of dissolved organic matter in the western tropical Pacific Ocean*. J. Geophys. Res.: Biogeosci. 125(3), e2019JG005425. https://doi.org/10.1029/2019JG005425

Zepp, R.G., Sheldon, W.M., Moran, M. A., 2004. *Dissolved organic fluorophores in southeastern US coastal waters: correction method for eliminating Rayleigh and Raman scattering peaks in excitation-emission matrices*. Mar. Chem. 89(1–4), 15–36. https://doi.org/10.1016/j.marchem.2004.02.006

Zhang, M., Wu, Y., Wang, F., Xu, D., Liu, S., Zhou, M., 2020. *Hotspot of organic carbon export driven by mesoscale eddies in the slope region of the northern South China Sea*. Front. Mar. Sci. 7, 444. https://doi.org/10.3389/fmars.2020.00444

Zhang, X., Chen, J., Xiang, L., Fang, J., Li, D., 2014. *A preliminary study on the characteristics of marine nepheloid layers in the northern South China Sea and their influential factors*. Acta Oceanol. Sin. 36(02), 51–65. https://doi.org/10.3969/j.issn.0253-4193.2014.02.006